Regular Article

PHYSICAL CHEMISTRY RESEARCH
Published by the
Iranian Chemical Society
www.physchemres.org
info@physchemres.org

***Phys. Chem. Res.**, Vol. 7, No. 2, 309-325, June 2019*
DOI: 10.22036/pcr.2019.158459.1567

TiO_2@$CoFe_2O_4$ Nanofiber for the Photocatalytic Degradation of Direct Red 80

S.S. Yasini Ardakani, R. Abghari* and M. Mirjalili
Department of Textile, Yazd Branch, Islamic Azad University, Yazd, Iran
(Received 24 November 2018, Accepted 18 February 2019)

Here, we report a significant enhancement in photo-activity of titanium dioxide by combination of $CoFe_2O_4$ and TiO_2 structure. First, $CoFe_2O_4$, TiO_2 and TiO_2@$CoFe_2O_4$ nanofibers were prepared *via* a combination of electrospinning method and in-situ polymerization. The morphology and crystalline structure of composite nanofibers were investigated using scanning electron microscopy (SEM) and X-ray diffraction, comprehensively. Because of the magnetic activity of $CoFe_2O_4$ ferrites, separation of the photocatalysts, after photo-oxidative process, is facilated in a medium of TiO_2@$CoFe_2O_4$. The photocatalytic activities of the nanofibers were conducted by photo-oxidative decomposition of Direct Red 80 (DR80). Furthermore, the influence of some parameters affecting on the dye removal including nanofiber dosage, initial dye concentration and solution pH were studied to gain a maximum degradation. The results confirmed that initial dye concentration has the highest impact on the photo-degradation of DR80. Among the synthesized samples, TiO_2@$CoFe_2O_4$ composite demonstrated much higher photocatalytic activity as well as initial degradation rate.

Keywords: Electrospinning method, TiO_2@$CoFe_2O_4$ nanofiber, Direct Red 80, Photocatalyst

INTRODUCTION

Textile dyes are most polluting compounds having the greatest impact on the environment. Over 50% of currently used dyes are Azo class which most of them have carcinogenic effects [1]. Further, under light irradiation, they have negative biological impacts on aquatic plants. Therefore, this kind of wastewater should be controlled to protect the ecosystem. Photo-decolorization (photocatalytic oxidation process) is an advanced method for degradation of organic pollutants [2-7]. Here are some of the main benefits of using this kind of technology: pollution-free storage (*i.e.*, solar energy), no disposal problem, elimination of a variety of hazardous organic compounds, as well as low cost. TiO_2 is one of the most promising/representative versatile oxide semiconductors extensively employed in many applications such as, photosplinting water, solar cell, sensors and especially in photo catalysis systems [8-11]. TiO_2 in anatase phase is a wide band gap semiconductor (3.2 eV) and electron-hole pairs are produced by irradiation of a beam light with energy greater than 3.2 eV (wave length smaller than 400 nm). They can follow to produce reactive oxygen species such as hydrogen peroxide, superoxide and hydroxyl radicals in aqueous solution (Eqs. (1)-(5)) which can play a main role to remove pollutants using oxidation process.

$$e^-_{CB} + O_2 \longrightarrow O_2^{\bullet -} \quad (1)$$

$$O_2^{\bullet -} + H^+ \longrightarrow HO_2^{\bullet} \quad (2)$$

$$HO_2^{\bullet} + O_2^{\bullet -} + H^+ \longrightarrow O_2 + H_2O_2 \quad (3)$$

$$H_2O_2 + e^-_{CB} \longrightarrow OH^- + HO^{\bullet} \quad (4)$$

$$OH^- + \text{hole} \longrightarrow HO^{\bullet} \quad (5)$$

Today, TiO_2 nanofibers have attracted great attention due to their larges specific surface area and chemical/mechanical

*Corresponding author. E-mail: abghariramin@iauyazd.ac.ir

stabilities. Electro-spinning is a relatively simple method to generate nanofibers of TiO_2 with controllable diameters and porous structures. Tek men *et al.* [12] successfully prepared TiO_2 nanofibers with a diameter of about 54-78 nm using a solution containing (PVP) and Ti-iso prop oxide with electro-spinning method. li and Xia [13] proposed the same procedure to control diameter of TiO_2 nanofibers in the range of 20-200 nm. Also many researches have focused on the technical method to combine TiO_2 nanofibers with other semiconductors. Recently, separation of TiO_2 nanoparticles from the suspension (with combination of magnetic particles) has been reported using coupled heterogeneous photocatalysis system [14].

The main types of magnetic compounds employed as photo-catalyst are ferrites with the empirical formula MFe_2O_4. The influence of different metal (M) such as Li, Mg, Ca, Ti, Co, Ni, Zn and Cd on morphology, structure and magnetic properties of ferrits has been investigated [15-17]. Among them, Co showed greater effect on photo catalytic activity as long as thermal and chemical stability in aqueous solution. Combination of two semiconductors is one of the technical methods to improve photo-activity using photo-generated electron-holes efficient separation [18-25]. Li *et al.* [26] prepared $TiO_2/CoFe_2O_4$ composite nanofibers with an average diameter of 110 nm successfully by sol-gel method and electrospinning technology. While both nanocomposits and nanofibers of $TiO_2/CoFe_2O_4$ showed a high photocatalytic activity for dye-degradation [18,19,26], the comparison between the combined semiconductor with the solitary ones, *i.e.*, TiO_2 and $CoFe_2O_4$, in the same synthesized and reaction conditions has been neglected yet. This may illuminate the combination effect on the photo-reaction mechanism based on charge separation especially. In general, the energetic positions of the valence and conduction band should be considered to get the next growth engine for the combined semiconductor industry. Therein, electron transfer from CB of photo-excited large band gap semiconductor to another one can extend the e-h life time and will make it possible to reach higher photo-activity. In the present research, photocatalytic activity of TiO_2 for azo-dye degradation in the presence of $CoFe_2O_4$ is investigated.

The present study is organized as follow: Experimental details including synthesis procedure, characterization methods, and photo-degradation evaluation of $TiO_2@CoFe_2O_4$ composite along with TiO_2 and $CoFe_2O_4$ nanofibers, which are given in section 2. Next, we describe the experimental results obtained from characterization instruments/techniques and also photo-degradation of Direct Red 80 (DR80), under UVA light illumination. Also, photo-degradation mechanism and reaction kinetic are explained in section 3 by detail. At the end of the paper, effect of operation parameters on dye removal such as initial pH levels, dye concentration and nanofiber dosage are being investigated. Central composite design (CCD) method is applied to gain optimal and the best conditions.

MATERIAL AND METHODS

Preparation of TiO_2, $CoFe_2O_4$ and $TiO_2@CoFe_2O_4$ Nanofibers

TiO_2 nanofiber was prepared from a precursor gel containing 2 g of PVP, 1 ml of Tetrabutyltitanate, 5 ml of acetic acid, and 25 ml of ethanol. $Cofe_2O_4$ nanofibers were synthesized by using 2 g of PVP, 2 g of $Fe(NO_3)_3.9H_2O$, 0.6 g of $Co(CH_3COO)_2.4H_2O$, 20 ml of ethanol, and 8 ml of H_2O. For $TiO_2@CoFe_2O_4$ nanofiber, TiO_2 precursor (including PVP) was gradually added into the $CoFe_2O_4$ precursor solution (without PVP). It should be mentioned that the mass ratio of TiO_2 to $CoFe_2O_4$ is about 1:2. As-prepared samples were stirred magnetically at 2000 rpm for 12 h. Then, electrospinning solution was loaded into a plastic tube (~9 mm in diameter). The distance between the spinneret tip and collector was set to 15 cm when a 18 kV step voltage was applied. The electrospun fibers were annealed at 80 °C for 12 h and then calcined in air environment at 550 °C for 3 h with heating and cooling rates of 2 °C min^{-1}.

Photocatalytic Activity Evaluation

The photocatalytic activity of the synthesized nanofibers was evaluated using a photo-decolourization of DR80 solution. In a typical experiment, 200 ml of aqueous DR80 solution was mixed with specific amount of the photocatalysts at a different pH and the mixture was stirred vigorously. The DR80 photo-degradation was carried out in a flask by a 125 W mercury lamp [1]. After a time interval (5 to 60 min), by the UV-Vis spectrophotometer (CECIL

Table 1. DOE Design Matrix for Photo-degradation of DR80 Based on Different Values of pH, Initial Dye Concentration and Nanofibers Dosage

Run	pH	Nanofiber dosage (ppm)	Dye concentration ($g\ ml^{-1}$)	Dye removal (%) by TiO_2	Dye removal (%) by $CoFe_2O4$	Dye removal (%) by $TiO_2/CoFe_2O_4$
1	9.1	100	0.006	78.6	74.66	88.9
2	2.1	100	0.004	60.04	56.08	70.5
3	5.6	120.5	0.005	75.9	71.89	86.1
4	2.1	40	0.004	85.33	81.36	86.35
5	11.4	70	0.005	73.48	69.25	83.7
6	5.6	70	0.0033	72.25	68.22	79.8
7	5.6	70	0.005	85.96	81.39	95.8
8	5.6	19.5	0.005	89.61	85.74	99.6
9	9.1	40	0.006	82.14	78.19	93.1
10	5.6	70	0.005	79.67	75.6	88.99
11	1.00	70	0.005	80.74	76.99	90.8
12	2.1	100	0.006	82.74	78.6	92.79
13	5.6	70	0.005	79.4	75.2	89.4
14	5.6	70	0.005	79.21	75.6	90.001
15	5.6	70	0.0066	80.15	76.5	90.15
16	5.6	70	0.005	79.88	75.7	89.96
17	2.1	40	0.006	85.6	81.5	95.6
18	9.1	40	0.004	50.78	46.9	60.8
19	9.1	100	0.004	49.66	45.5	59.7

2021), the concentration of the remaining color in supernatant solution was determined. The pH of the flask solution was adjusted to a desired value by adding 0.1 M NaOH or 0.1 M HCl in a droplet.

Design of Experiments (DOE)

A design expert toolbox and the engineering tools of the response surface methodology were applied to optimize the photo-degradation conditions of DR80 dye. There were three independent variables including values of pH, initial dye concentration and nanofibers dosage (Table 1). The effects of these variables on the photo-degradation of DR80 solution dye were evaluated.

RESULT AND DISCUSSION

Characterization

In the present research, the as-prepared samples were

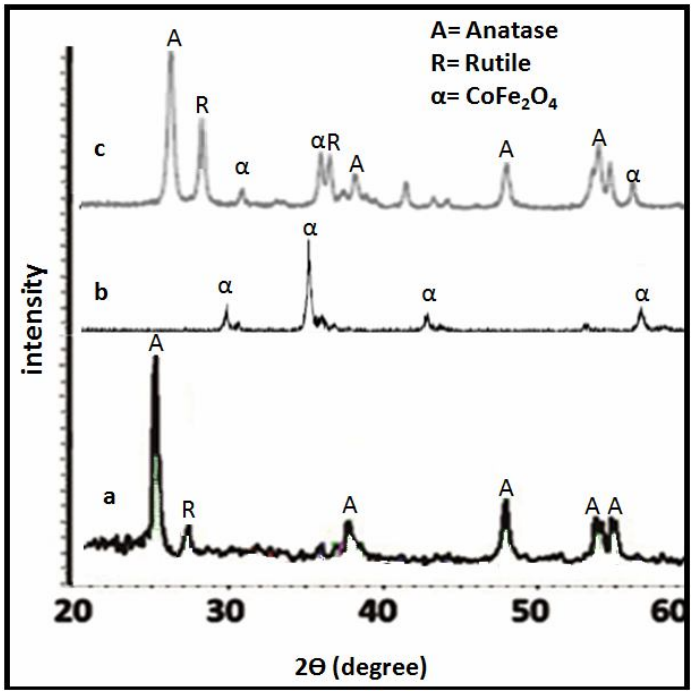

Fig. 1. XRD patterns of (a) TiO_2, (b) $CoFe_2O_4$ and (c) TiO_2@$CoFe_2O_4$ nanofibers.

investigated using XRD, BET, DRS and SEM instruments, in detail. The XRD spectra of the samples revealed that the presence of anatase and rutile phases of TiO_2 in the titania based nanofibers (Fig. 1). All XRD patterns represent the crystalline nature of the samples and also indicate the presence of anatase phase (JCPDS card No. 00-021-1272) as expected for TiO_2 annealed at this temperature. The diffraction peaks in XRD spectrum are attributed to the spinel $CoFe_2O_4$ crystalline phase, in the form of $CoFe_2O_4$ and TiO_2@$CoFe_2O_4$, resulted from combination of TiO_2 and $CoFe_2O_4$.

SEM images of the as-prepared photocatalysts (Fig. 2) represent the fair morphology of the nanofibers as long as uniform diameter of less than 100 nm. The results are in accordance with the previous results [19]. Herein, the as synthesized nanofibers exhibit length up to several millimeters with smooth surface.

Photo Catalytic Degradation

Effect of catalysts dosage. Figure 3a shows photo-catalytic dye degradation using different amounts of TiO_2 nanofibers. Photo-decolorization is mostly performed in the first 10 min for the samples. It can be seen that the dye degradation increases with an increase in nanofiber dosage limitedly up to a threshold. Photo-catalytic activity does not improve noticeably by increasing the concentration of the sample from 0.004 to 0.006 g. It can be explained by more aggregation of the active sites by increasing the amount of the catalysts. Figures 3b and c represent dye removal with different dosages of $CoFe_2O_4$ and TiO_2@$CoFe_2O_4$ nanofibers, respectively. The results introduce 0.004 g of the catalysts and irradiation time of about 10 min as preferred conditions. On the other hand, combination of semiconductors (*i.e.*, TiO_2@$CoFe_2O_4$) exhibited more photocatalytic activity in degradation reactions. For example, at the case of optimal condition (0.004 g concentration and 10 min irradiation), dye removal values for TiO_2/$CoFe_2O_4$ composite, $CoFe_2O_4$ and TiO_2 nanofibers were about 80%, 60% and 40%, respectively (Fig. 3d).

Effect of pH. The effect of pH on DR80 elimination in the presence of synthesized photocatalysts is illustrated in Fig. 4. The results show that pH plays a significant role on removal process of DR80 at the aqueous solution for all types of catalysts. It means that DR80 as a direct dye

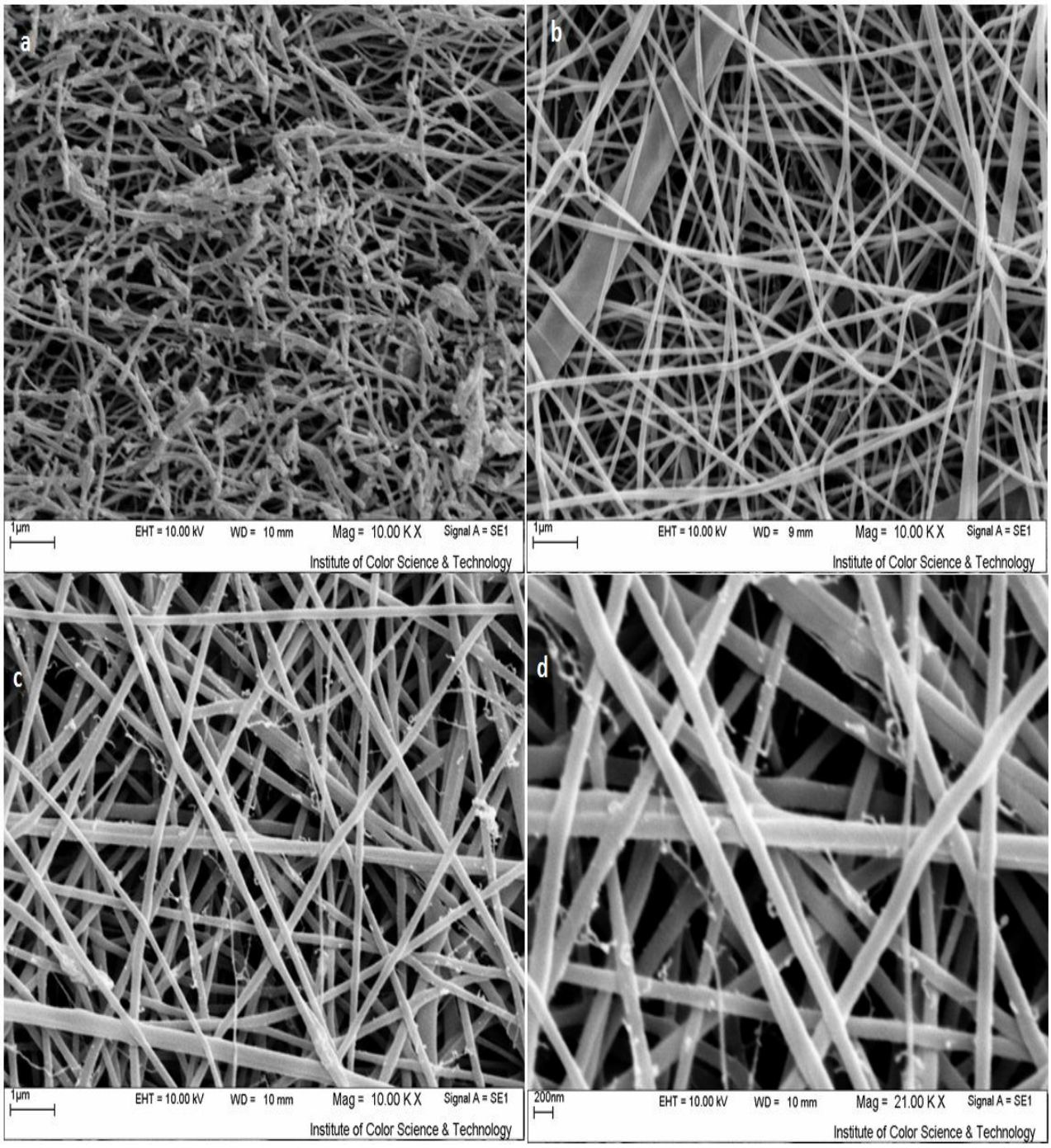

Fig. 2. SEM images of (a) TiO_2, (b) $CoFe_2O_4$, and (c,d) TiO_2@$CoFe_2O_4$ nanofibers.

adsorbed on different sites and also shows that the dye removal decreases in pH > 7, dramatically. For the synthesized nanofibers in aqueous solution, with hydroxyl group on the surface, surface charges varied from OH^{2+}, OH to O^- with increasing pH. In a dye solution with higher pH values, the surface of adsorbents bears negative charges

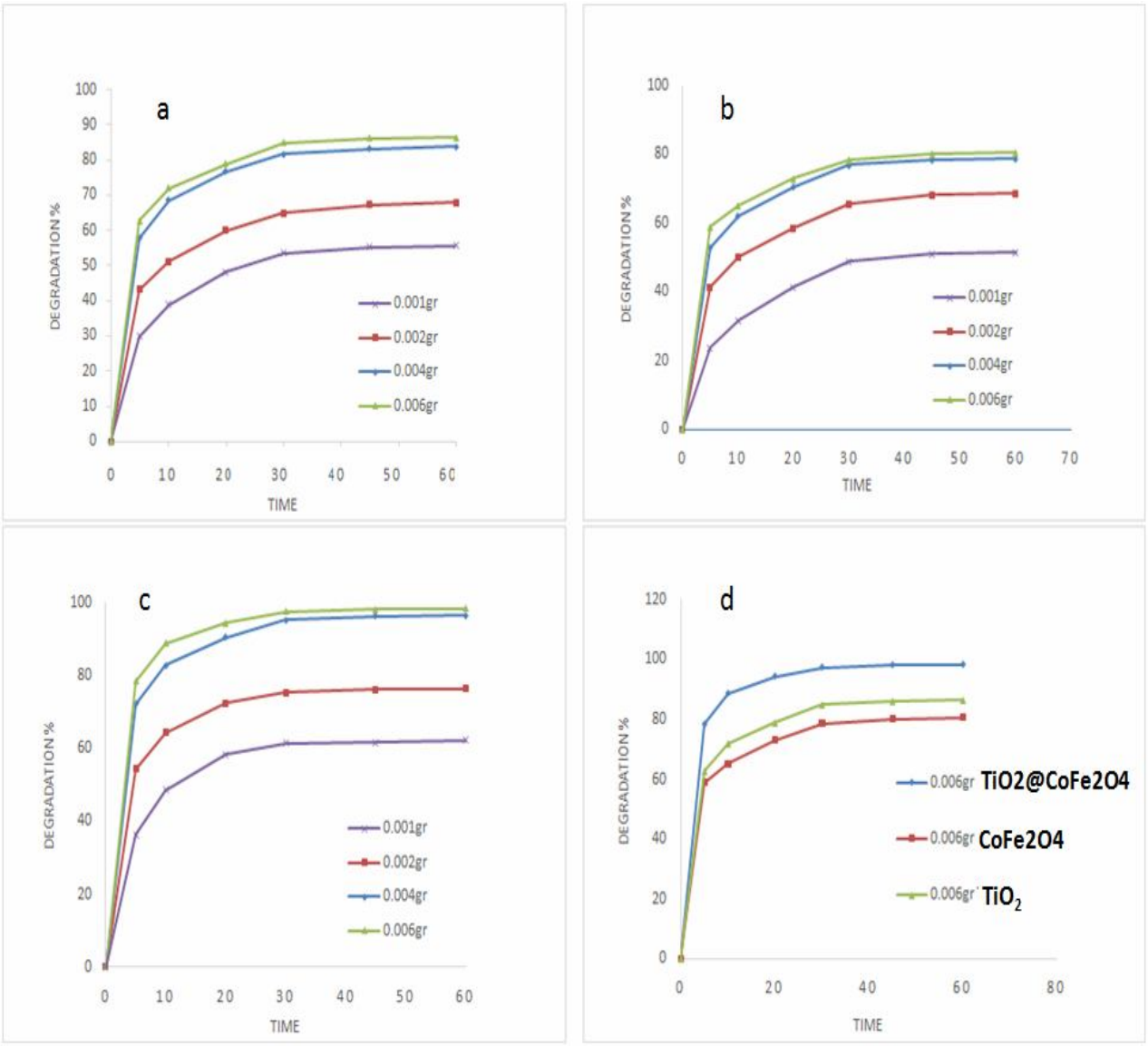

Fig. 3. Effect of (a) TiO_2, (b) $CoFe_2O_4$ and (c) TiO_2@$CoFe_2O_4$ nanofibers dosage on dye removal.

whereas it has positive charge at the lower pH. Therefore, an increment in pH of solution does not favor the adsorption of anionic dye due to the electrostatic repulsion. Dye removal at the optimum pH (pH = 2.1) is presented in Fig. 4d. The experimental results confirm that TiO_2@$CoFe_2O_4$ sample has greater activity than the other nanofibers.

Effect of initial dye concentration. The ability of photo degradation of DR80 using different initial concentrations of the as synthesized nanofibers are presented in Fig. 5. As expected, dye removal percentage decreased by increasing the initial dye concentration. Obviously, higher initial value of dye concentration shows lower ratio of available active sites per molecule and also higher molecules repulsion. It means that dye adsorption, as the first step, has a main effect on photo-degradation process. The initial dye concentration can affect the diffusion of light from the solution. When the light penetration is declined, less

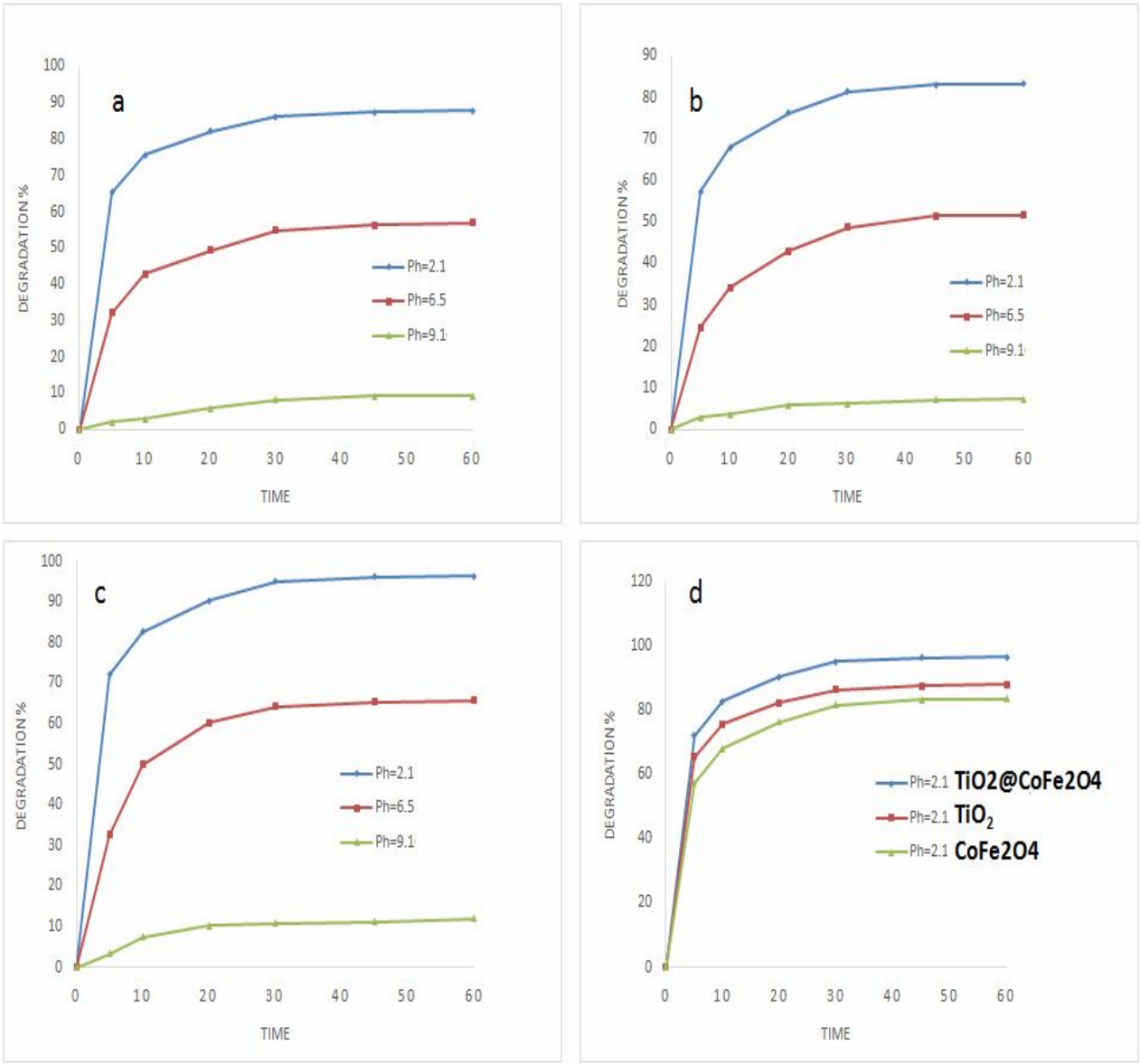

Fig. 4. Effect of pH on dye removal by (a) TiO_2, (b) $CoFe_2O_4$, and (c) TiO_2@$CoFe_2O_4$ nanofibers.

photons reach the photocatalyst surface [27-29]. Hence, dye molecules and photocatalyst surface compete for light absorption. Initial concentration shows more effect on the $CoFe_2O_4$ catalytic efficiency. Herein, dye removal percentage changes from 83.4% to 49.6% for 40 and 100 ppm of initial concentration of DR80. This value is changing from 96.4-61.4% for TiO_2@$CoFe_2O_4$ sample and 87.9-57.1% for TiO_2 nanofibers.

Photo-degradation Mechanism and Reaction Kinetic

Photo-catalytic degradation of DR80 and its decolourization chemistry were kinetically analyzed based on Langmuir-Hinshelwood equations [9]. A rate equation for heterogeneous photo-degradation was derived where initial rate (r) and dye concentration can be described as follows:

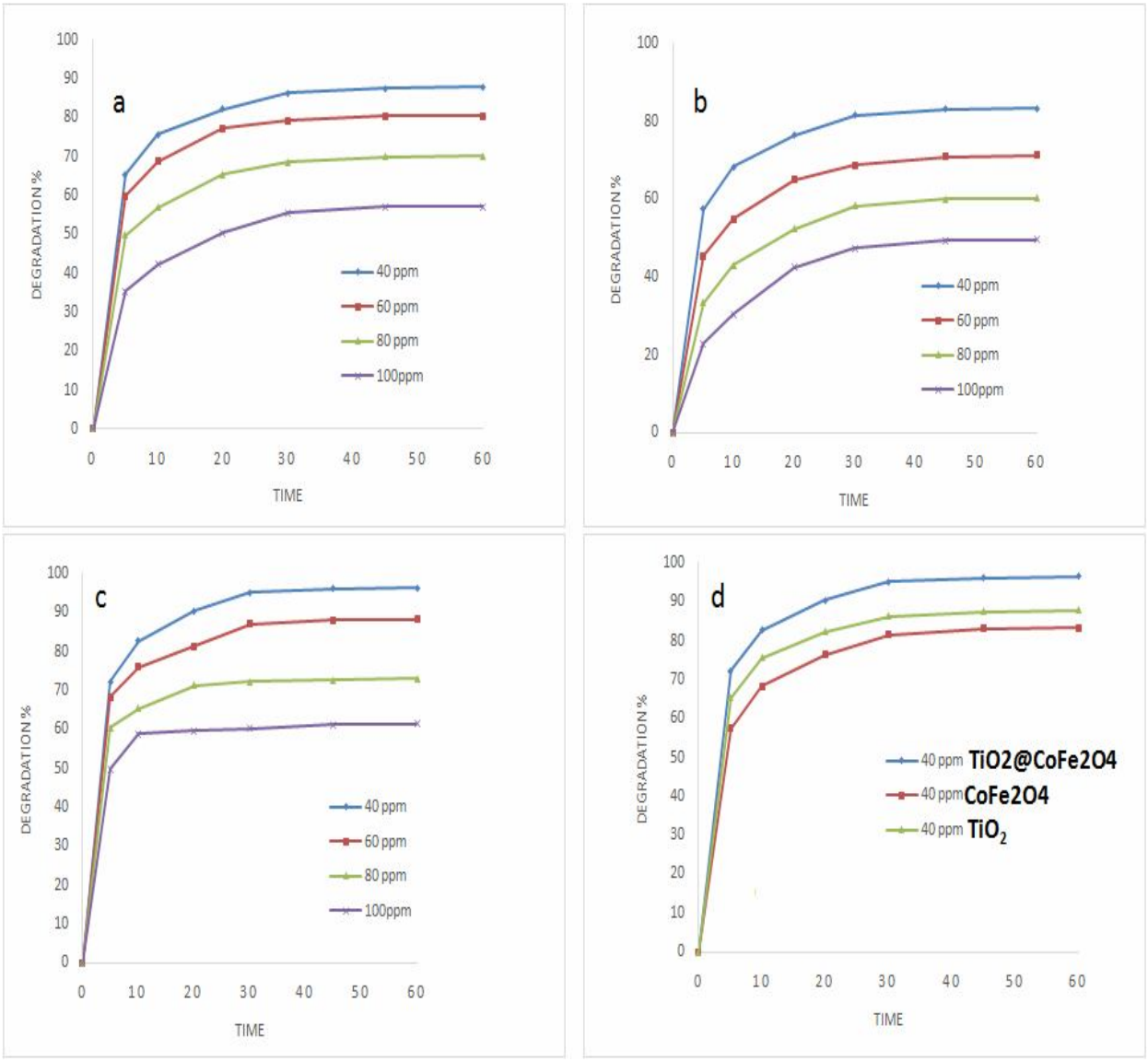

Fig. 5. Effect of initial dye concentration on dye removal by (a) TiO_2, (b) $CoFe_2O_4$ and (c) TiO_2@$CoFe_2O_4$ nanofibers.

$$r = \frac{-dc}{dt} = K_{obs} C \rightarrow \ln \frac{C_t}{C_0} = -K_{obs} t$$

C_0 (ppm) and C_t (ppm) represent initial and final dye concentrations in photo-degradation catalytic process before and after irradiation, respectively. Table 2 shows the calculated values for K_{obs} (reaction rate coefficient) obtained from plotting points of $\ln C_t/C_0$ *vs.* irradiation time.

At the next stage, the adsorption coefficient (K_{ads}) and pseudo first-order rate constant (k) were calculated according to the following relations:

$$\frac{kK_{ads}C}{1+K_{ads}C} = K_{obs} \rightarrow \frac{1}{K_{obs}} = \frac{1}{kK_{ads}} + \frac{C}{k}$$

From the reported results in Table 2, it can be cocluded that the initial degradation rates of TiO_2@$CoFe_2O_4$ nanofibers are much higher than the other samples, although, the

Table 2. Values of Initial Concentrations of DR80 (C_0), Initial Degradation Rate Coefficient (K_{obs}), Adsorption Coefficient (K_{ads}), and Pseudo First-order Rate Constant (k) for as-prepared Nanofibers

Nanofibers	C_0 of DR80 (ppm)	K_{obs} (h^{-1})	K_{ads} (ppm^{-1})	BET surface area ($m^2\ g^{-1}$)	K (ppm h^{-1})
$CoFe_2O_4$	40	1.47	0.41	19.6	63.29
	60	1.01			
	80	0.78			
	100	0.61			
TiO_2	40	1.68	0.53	23.5	68.96
	60	1.24			
	80	0.92			
	100	0.68			
TiO_2@$CoFe_2O_4$	40	2.25	0.49	21.7	93.45
	60	1.49			
	80	1.12			
	100	0.92			

adsorption coefficient and the BET surface area of theas-synthesized nanofibers are almost identical. It means that compound semiconductors reveal more photo-activity than the other single-component photocatalysts.

The direct band-gaps of the composite nanofiber was obtained from the intercept of the graphs drawn for $(\alpha\ h\nu)^2$ *vs.* $h\nu$ (Fig. 6), where, α and $h\nu$ are the absorption coefficient and photon energy, respectively [27,29]. Here, we obtained the direct band gap of 1.1 eV for TiO_2@$CoFe_2O_4$ nanofibers in line with the previous result [18].

The proposed reaction mechanism for a heterojunction structure is described according to the descriptive scheme shown in Fig. 7 as follows: $CoFe_2O_4$ bulk has a direct band gap of about 1.1 eV which is smaller than the TiO_2 (3.20 eV) [4]. Its conduction band is less anodic than the corresponding TiO_2 band, and $CoFe_2O_4$ valence band is more cathodic than the TiO_2 valence band. Electron/hole pairs are produced in the TiO_2@$CoFe_2O_4$ nanofibers by irradiation and then the photogenerated electrons on the TiO_2 conduction band are injected into the $CoFe_2O_4$ conduction band. Created holes on the TiO_2 valence band may be transferred to the upper valence band of $CoFe_2O_4$.

Generally speaking, in the case of compound semiconductor, the recombonation rate of photogenerated electrons and holes decreases which can affects on photocatalyst's life time and its photocatalytic activity.

Statistical Analysis

The response surface methodology (RSM) and central composite design (CCD) were used to optimize the experimental condition for the photo-degradation process [30]. The whole CCD consists of a total of 19 experiments (Table 1). The modeling experiments targeted the value of degradation percentage for all synthesized nanofibers. The pH, initial dye concentration and nanofibers dosage as

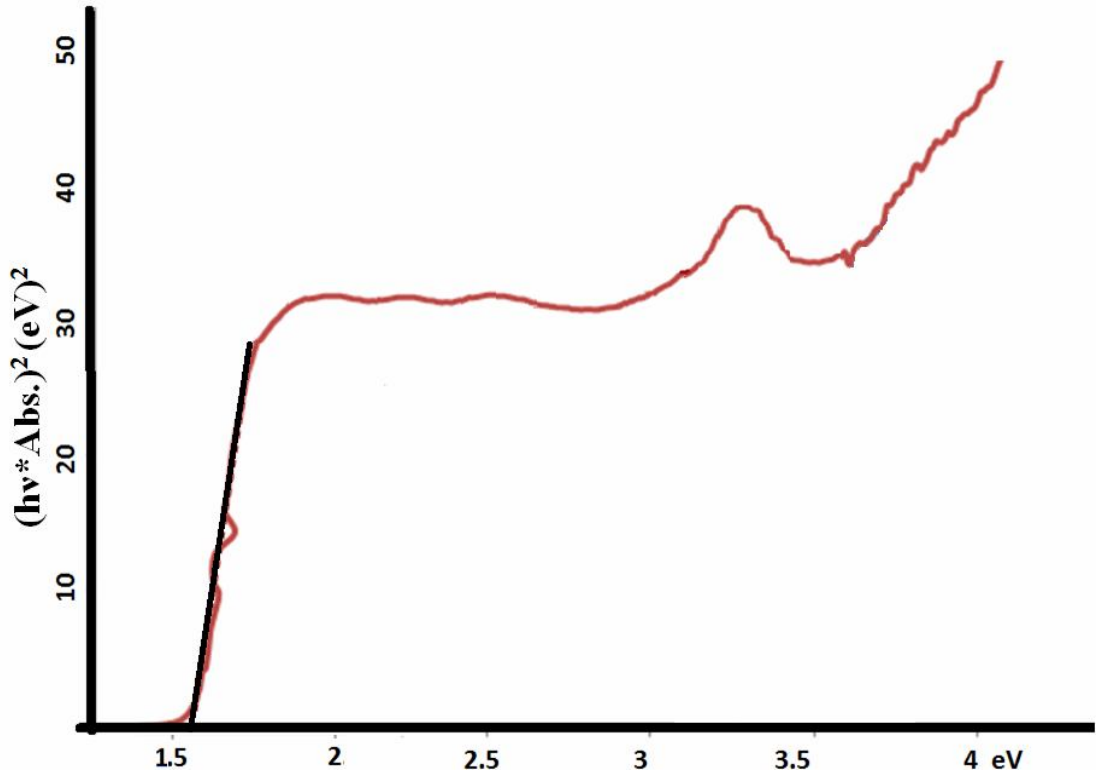

Fig. 6. UV-Vis DRS graphs in terms of (hv ×Ads.)^2 *versus hv* for TiO_2@$CoFe_2O_4$ nanofiber.

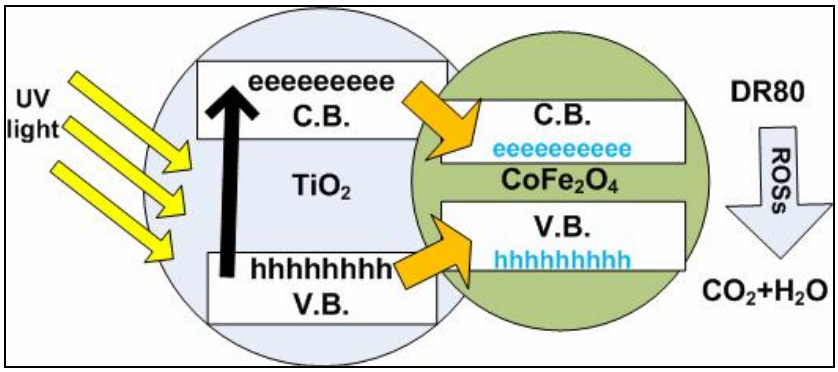

Fig. 7. Schematic illustration of the proposed mechanism for photo-degradation of DR80 over TiO_2@$CoFe_2O_4$ Nanofibers.

independent variables and photo-degradation percent as dependent variables were introduced. On the basis of the results obtained from the surface plots and the independent variables, mathematic equations for TiO_2, $CoFe_2O_4$ and TiO_2@$CoFe_2O_4$ were presented as follows.

Dye degradation by TiO_2 = +81.08 - 4.74 × A - 4.09 × B + 11.89 × C + 2.94 × A × B + 7.85 × A × C + 4.21 × B × C - 2.74 × A^2 - 0.75 × B^2 - 8.66 × C^2

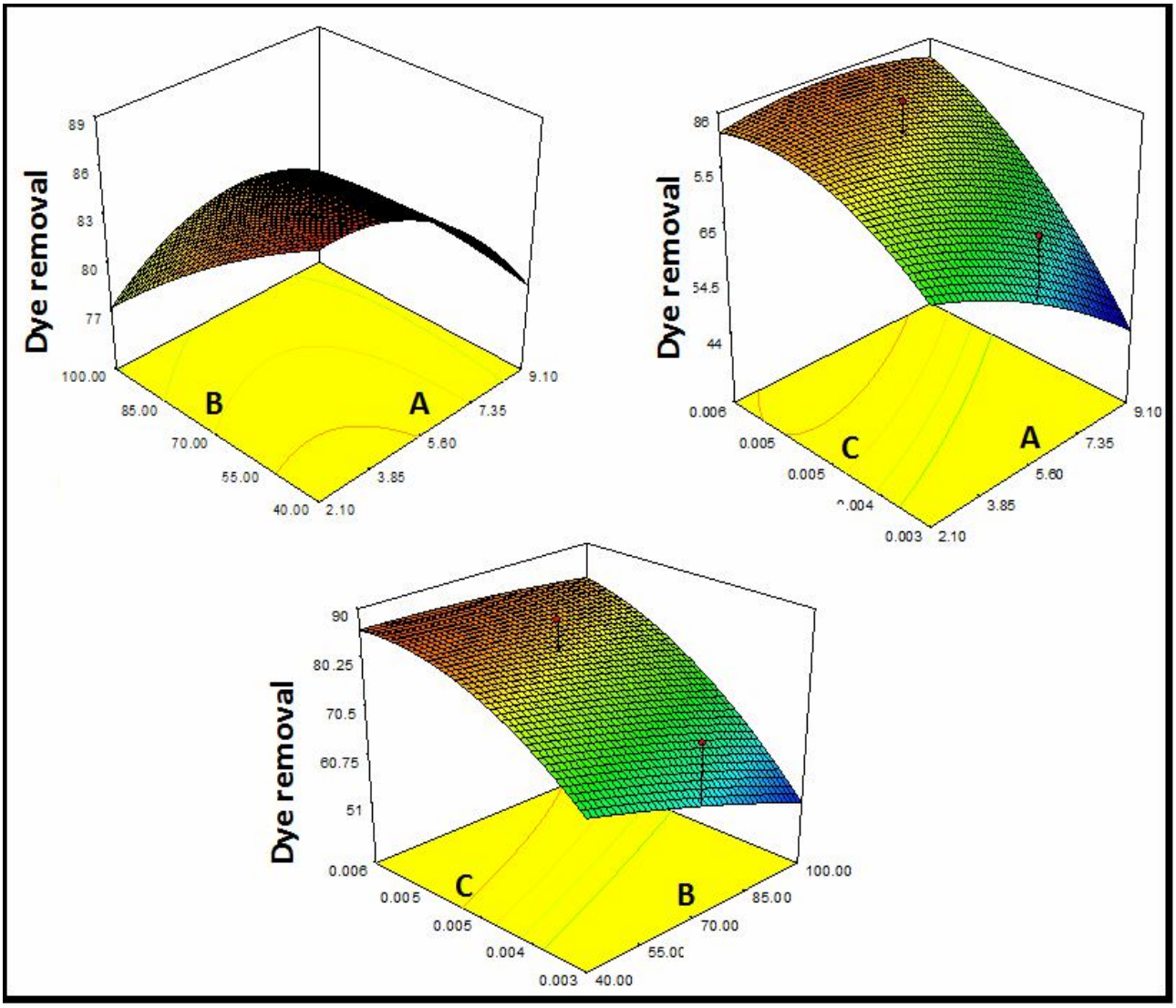

Fig. 8. 3D graphs for the response surface of the dye removal activity of TiO_2 nanofibers affected by pH (A), nanofiber dosage (B) and initial dye concentration (C).

Dye degradation by $CoFe_2O_4$ = +76.96 - 4.78 × A - 4.13 × B + 11.95 × C + 2.91 × A × B + 7.94 × A × C + 4.26 × B × C - 2.71 × A^2 - 0.70 × B^2 - 8.44 × C^2

Dye degradation by TiO_2/$CoFe_2O_4$ = +91.11 - 4.00 × A - 3.42 × B + 13.60 × C + 1.67 × A × B + 6.30 × A × C + 2.09 × B × C - 2.81 × A^2 - 0.83 × B^2 - 10.22 × C^2

where A, B and C are pH, nanofiber dosage and initial dye concentration, respectively. The maximum dye removal of 89.61%, 85.74% and 99.60% can be obtained by optimal samples of TiO_2, $CoFe_2O_4$ and TiO_2@$CoFe_2O_4$ nanofibers, respectively. The optimal value/situation can be obtained under pH, nanofiber dosage and initial dye concentration values of 2.46, 99.97 ppm and 0,01 g l^{-1}, respectively. Figures 8-10 show the 3D graphs for the response surface of the dye removal activity of nanofibers affected by pH (A), nanofiber dosage (B) and initial dye concentration (C). They

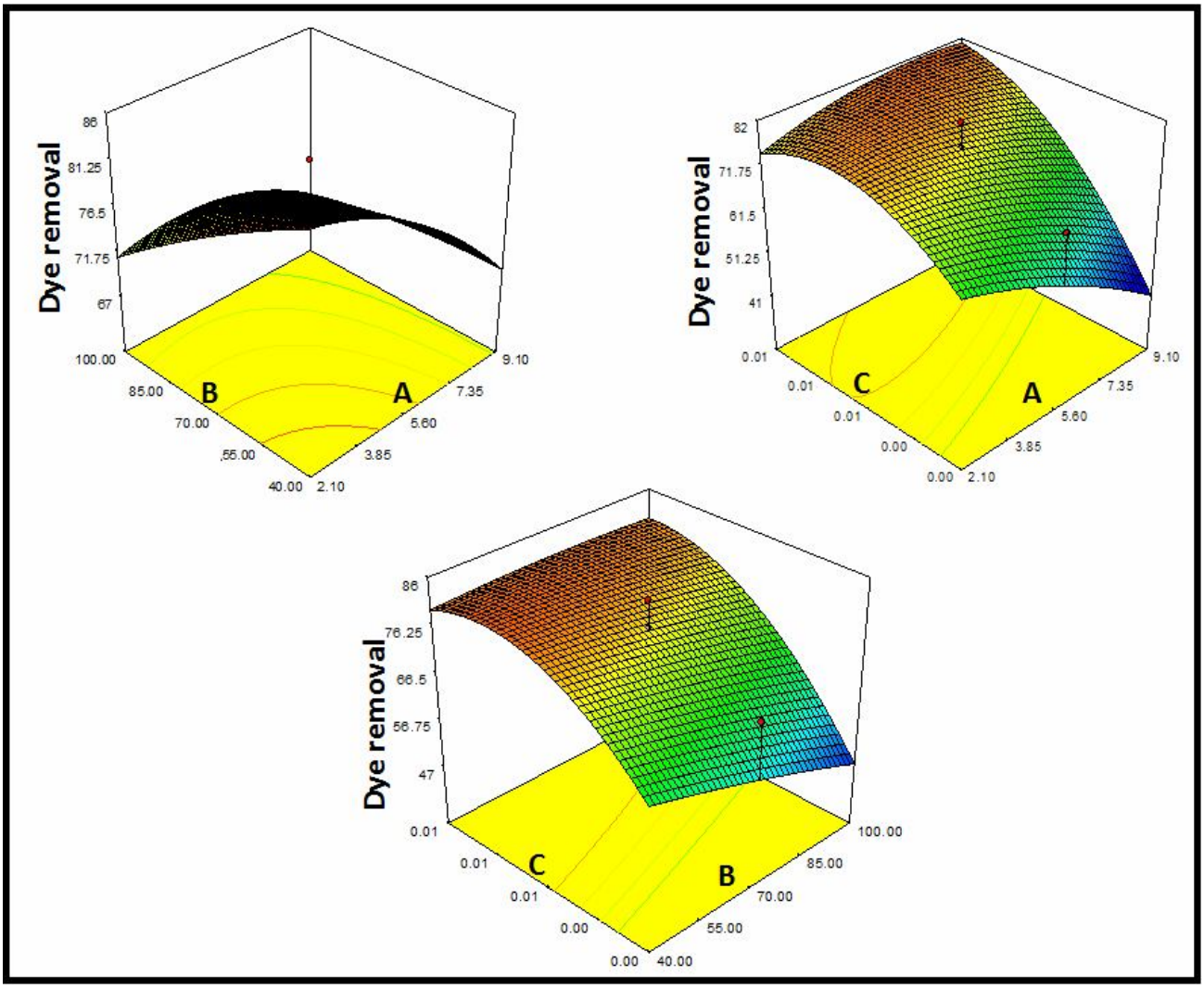

Fig. 9. 3D graphs for the response surface of the dye removal activity of $CoFe_2O_4$ nanofibers affected by pH (A), nanofiber dosage (B) and initial dye concentration (C).

showed that for all nanofibers, when the pH is at its lowest value (2.10), dye degradation decreases/increases with the increase in the initial dye concentration/nanofiber dosage.

Based on the validity of the test designed by RSM, the P value was lower than 0.05 for all nanofibers (according to the Tables 3-5). Therefore, it can be concluded that there is a significant difference between the effects of the variables on the dye removal by the synthesized nanofibers. In addition, given that the F value of initial dye concentration is higher than that of the proposed model, initial dye concentration has the highest influence on the photo-degradation of DR80.

CONCLUSIONS

In the present study, TiO_2, $CoFe_2O_4$ and TiO_2@$CoFe_2O_4$ composite nanofibers with pore diameter of less than 100 nm were prepared by combination of in-situ polymerization and electrospinning technology, successfully. The structural analysis confirms the presence of either anatase and rutile

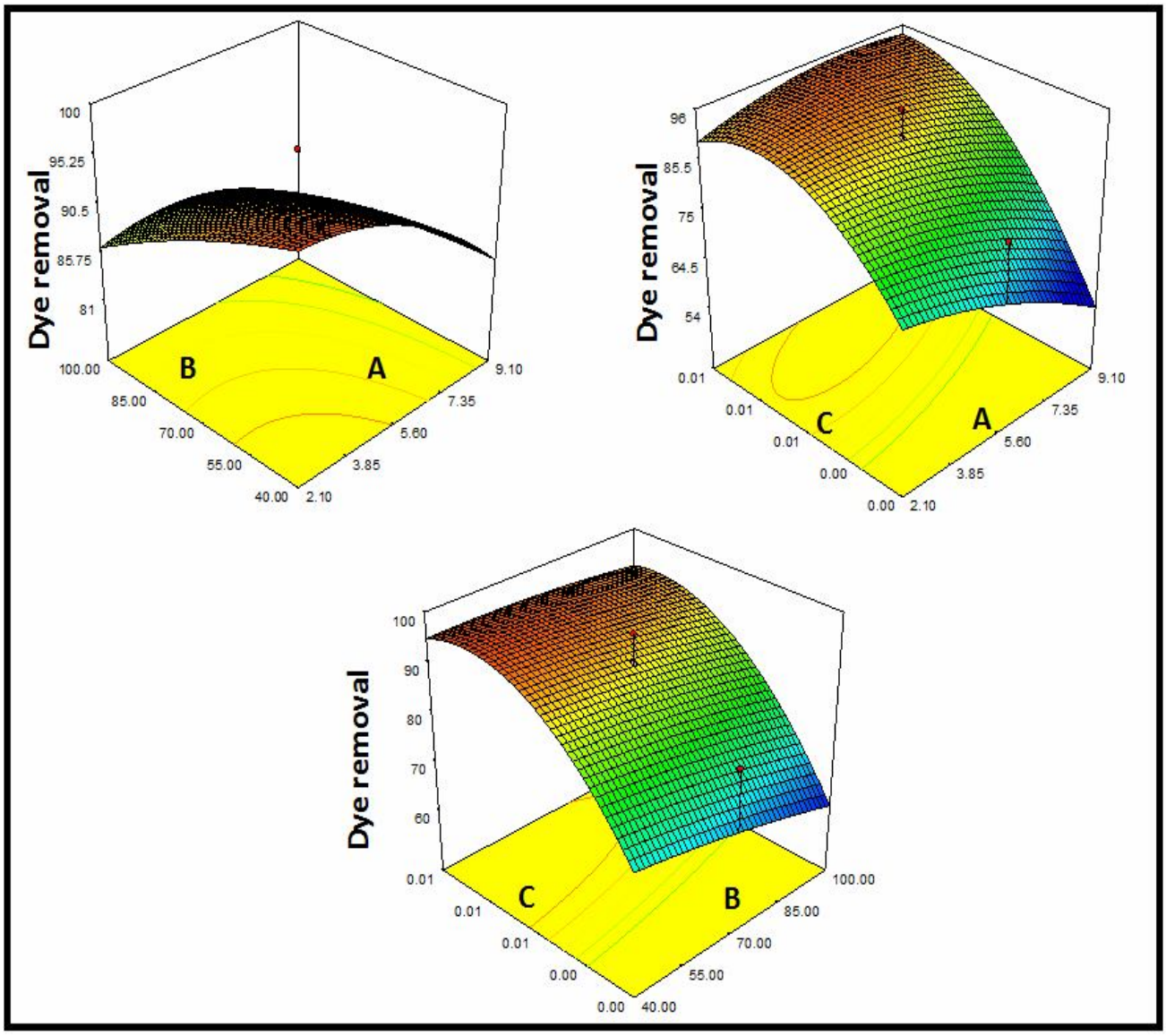

Fig. 10. 3D graphs for the response surface of the dye removal activity of TiO_2@$CoFe_2O_4$ nanofibers affected by pH (A), nanofiber dosage (B) and initial dye concentration (C).

phases in TiO_2 structure as long as spinel $CoFe_2O_4$ phase. Synthesized nanofibers were considered to remove DR80 under illumination of UV-Vis light. Photo-degradation experiments showed the highest efficiency at pH 2.1. Also, combined photocatlyst (TiO_2@$CoFe_2O_4$) exhibited higher photocatalytic degradation efficiency of DR80 than the other nanofibers. The results of statistical analysis showed that initial dye concentration has the highest and meaningful effect on the photo-degradation process. Kinetic study of the photo-catalytic degradation revealed that the initial degradation rates of TiO_2@$CoFe_2O_4$ nanofibers are much higher than those for the other nanofibers. Based on the above results, the TiO_2@$CoFe_2O_4$ nanofibers show better photocatalytic activity than that of the single component semiconductors under light exposure.

Table 3. ANOVA Results for Photo-degradation of DR80 by TiO_2 Nanofiber

ANOVA for response surface quadratic model					
Source	Sum of squares	df	Mean square	F Value	p-value Prob > F
Model	1712.626	9	190.2918	3.211455	0.0486
A-Ph	306.8967	1	306.8967	5.179336	0.0489
B-Concentration	228.542	1	228.542	3.856983	0.0811
C-Dye dosage	682.6683	1	682.6683	11.52104	0.0079
AB	68.97251	1	68.97251	1.164013	0.3087
AC	174.1911	1	174.1911	2.939732	0.1206
BC	50.05001	1	50.05001	0.844668	0.3820
A^2	102.5678	1	102.5678	1.730983	0.2208
B^2	7.58353	1	7.58353	0.127983	0.7288
C^2	128.0583	1	128.0583	2.161172	0.1756
Residual	533.2866	9	59.25407		
Lack of fit	500.0525	5	100.0105	12.03709	0.0159
Pure error	33.23412	4	8.30853		
Cor total	2245.913	18			

Table 4. ANOVA Results for Photo-degradation of DR80 by $CoFe_2O_4$ Nanofiber

ANOVA for response surface quadratic model					
Source	Sum of squares	df	Mean square	F Value	p-value Prob > F
Model	1725.856	9	191.7617	3.331761	0.0438
A-Ph	312.2984	1	312.2984	5.426025	0.0448
B-Concentration	232.9438	1	232.9438	4.047278	0.0751
C-Dye dosage	689.4595	1	689.4595	11.979	0.0071
AB	67.57031	1	67.57031	1.173999	0.3068
AC	178.5105	1	178.5105	3.101528	0.1121
BC	51.25781	1	51.25781	0.890578	0.3700
A^2	100.598	1	100.598	1.747838	0.2188
B^2	6.712183	1	6.712183	0.116621	0.7406
C^2	121.4983	1	121.4983	2.11097	0.1802
Residual	518.0009	9	57.55566		
Lack of fit	490.3349	5	98.06697	14.17866	0.0118
Pure error	27.66608	4	6.91652		

Table 5. ANOVA Results for Photo-degradation of DR80 by TiO_2@$CoFe_2O_4$ Nanofiber

ANOVA for response surface quadratic model					
Source	Sum of squares	df	Mean square	F Value	p-value Prob > F
Model	1669.206	9	185.4673	3.26035	0.0466
A-Ph	218.9364	1	218.9364	3.848707	0.0814
B-Concentration	159.4473	1	159.4473	2.802941	0.1284
C-Dye dosage	893.211	1	893.211	15.70186	0.0033
AB	22.3112	1	22.3112	0.392211	0.5467
AC	112.2002	1	112.2002	1.97238	0.1938
BC	12.35045	1	12.35045	0.21711	0.6523
A^2	107.7619	1	107.7619	1.894359	0.2020
B^2	9.399562	1	9.399562	0.165236	0.6939
C^2	178.2914	1	178.2914	3.134204	0.1104
Residual	511.9713	9	56.8857		
Lack of fit	480.3957	5	96.07915	12.17134	0.0156
Pure error	31.57554	4	7.893885		
Cor total	2181.177	18			

REFERENCES

[1] Elahifard, M. R.; Gholami, M. R., Acid blue 92 photocatalytic degradation in the presence of scavengers by two types photocatalyst, *Environ. Prog. Sus. Energy.* **2012**, *31*, 371-378, DOI: 10.1002/ep.10558.

[2] Kimiagar, S., Hydrophilicity and antibacterial properties of Ag/TiO_2 nanoparticle, *Phys. Chem. Res.* **2013**, *1*, 126-133, August, DOI: 10.22036/pcr.2013.3223.

[3] Elahifard, M. R.; Rahimnejad, S.; Haghighi, S.; Gholami, M. R., Apatite-coated Ag/AgBr/TiO_2 visible-light photocatalyst for destruction of bacteria, *J. Am. Chem. Soc,* **2007**, *129*, 9552-9553, DOI: 10.1021/ja072492m.

[4] Elahifard, M. R.; Ahmadvand, S.; Mirzanejad, A., Effects of Ni-doping on the photo-catalytic activity of TiO_2 anatase and rutile: Simulation and experiment, *Mat. Sci. Semicon. Proc.,* **2018**, *84*, 10-16, DOI: 10.1016/j.mssp.2018.05.00.

[5] Padervand, M.; Salari, H.; Ahmadvand, S.; Gholami, M. R., Removal of an organic pollutant from waste water by photocatalytic behavior of AgX/TiO_2 loaded on mordenite nanocrystals, *Res. Chem. Intermed.* **2012**, *38*, 1975-1985, DOI: 10.1007/s11164-012-0519-8.

[6] Elahifard, M. R.; Padervand, M.; Yasini, S.; Fazeli, E., The effect of double impurity cluster of Ni and Co in TiO_2 bulk; a DFT study, *J. Electroceram.* **2016**, *37*, 4536-4544, DOI: 10.1007/s10832-016-0027-0.

[7] Lykhin, A. O.; Ahmadvand, S.; Varganov, S. A., Electronic transitions responsible for C60+diffuse interstellar bands, *J. Phys. Chem Lett.* **2019**, *10*, 115-120, DOI: 10.1021/acs.jpclett.8b03534.

[8] Ricker, J. D.; Mohammadrezaei, V.; Crippen, T. J.; Zell, A. M.; Geary, L. M., Nitrous oxide promoted pauson-khand cycloadditions, organometallics, **2018**,

37, 4556-4559, DOI: 10.1021/acs.organomet. 8b00810.

[9] Elahifarda, M. R.; Vatan Meidanshahib, R., Photo-deposition of Ag metal particles on Ni-doped TiO_2 for photocatalytic application, *Prog. React. Kinet. Mech.* **2017**, *42*, 244-250, DOI: 10.3184/ 146867817x14821527549130.

[10] Elahifard, M. R.; Rahimnejad, S.; Pourbaba, R.; Haghighi, S.; Gholami, M. R., Photocatalytic mechanism of action of apatite-coated Ag/AgBr/TiO_2 on phenol and Escherichia coli and Bacillus subtilis bacteria under various conditions, *Prog. React. Kinet. Mech.* **2011**, *36*, 38-52, DOI: 10.3184/ 146867810X12925913885187.

[11] Esfandfard, S. M.; Elahifard, M. R.; Behjatmanesh-Ardakanii, R.; Kargara, H., DFT study on oxygen-vacancy stability in rutile/anatase TiO_2: Effect of cationic substitutions, *Phys. Chem. Res.,* **2018**, *6*, 547-563, DOI: 10.22036/pcr.2018.128713.1481.

[12] Tekmen, C.; Cocen, A. S. U., Titania nanofibers prepared by electrospinning, *Mater. Lett.,* **2008**, *62*, 4470-4472, DOI: 10.1016/j.matlet.2008.08.002.

[13] Li, D.; Xia, Y., Fabrication of titania nanofibers by electrospinning, *Nano Lett.,* **2003**, *3*, 555-560, DOI: 10.1021/nl034039o.

[14] Liu, S. Q., Magnetic semiconductor nano-photocatalysts for the degradation of organic pollutants, *Environ. Chem. Lett.* **2012**, *10*, 209-216, DOI: 10.1007/s10311-011-0348-9.

[15] Mishra, D.; Senapati, K. K.; Borgohain, C.; Perumal, A., $CoFe_2O_4$-Fe_3O_4 Magnetic nanocomposites as photocatalyst for the degradation of methyl orange dye, *J. Nanotechnol.,* **2012**, *ID 323145*, 6 pages, DOI: 10.1155/2012/323145.

[16] Moosavi, S. M.; Molla-Abbasi, P.; Haji-Aghajani, Z., Photo-catalyst $CoFe_2O_4$-TiO_2: Application in photo-degradation of organic dyes and magnetic nanocomposite preparation, *J. Mater. Sci: Mater. Electron.,* **2016**, *27*, 4879-4886, DOI: 10.1007/ s10854-016-4371-2.

[17] Hwangbo, Y.; Yoo, J. H.; Lee, Y. I., Electrospun $CoFe_2O_4$ nanofibers as high capacity anode materials for Li-ion batteries, *J. Nanosci. Nanotechnol.,* **2017**, *17*, 7632-7635, DOI:10.1166/jnn.2017.14763.

[18] Sathishkumar, P.; Mangalaraja, R. V.; Anandan, S.; Ashokkumar, M., $CoFe_2O_4$/TiO_2 nanocatalysts for the photocatalytic degradation of reactive red 120 in aqueous solutions in the presence and absence of electron acceptors, *Chem. Eng. J.,* **2013**, *220*, 302-310, DOI: 10.1016/j.cej.2013.01.036.

[19] Li, C. U.; Wang, J. N.; Wang, B.; Gong, J. R.; Lin, Z., Direct formation of reusable TiO_2/$CoFe_2O_4$ heterogeneous photocatalytic fibers *via* two-spinneret electrospinning, *J. Nanosci. Nanotechnol.* **2012**, *12*, 1-7, DOI: 10.1166/jnn.2012.5812.

[20] Fu, W.; Yang, H.; Li, M.; Li, M.; Yang, N.; Zou, G., Anatase TiO_2 nanolayer coating on cobalt ferrite nanoparticles for magnetic photocatalyst, *Mater. Lett.,* **2005**, *59*, 3530-3534, DOI: 10.1016/ j.matlet.2005.06.071.

[21] Liang, M.; Borjigin, T.; Zhang, Y.; Liu, B.; Liu, H.; Guo, H., Controlled assemble of hollow heterostructured g-C_3N_4@CeO_2 with rich oxygen vacancies for enhanced photocatalytic CO_2 reduction, *Appl. Catal. B: Environ.,* **2019**, *243*, 566-575, DOI: 10.1016/j.apcatb.2018.11.010.

[22] Ma, X.; Xiang, Q.; Liao, Y.; Wen, T.; Zhang, H., Visible-light-driven CdSe quantum dots/graphene/ TiO_2 nanosheets composite with excellent photocatalytic activity for E. coli disinfection and organic pollutant degradation, *Appl. Surf. Sci.,* **2018**, *457*, 846-855, DOI: 10.1016/j.apsusc.2018.07.003.

[23] Xia, Y.; Li, Q.; Lv, K.; Li, M., Heterojunction construction between TiO_2 hollowsphere and $ZnIn_2S_4$ flower for photocatalysis application, *Appl. Surf. Sci.,* **2017**, *398*, 81-88, DOI: 10.1016/j.apsusc.2016.12.006

[24] Li, Y.; Feng, X.; Lu, Z.; Yin, H.; Liu, F.; Xiang, Q., Enhanced photocatalytic H_2-production activity of C-dots modified g-C_3N_4/TiO_2 nanosheets composites, *J. Colloid. Interface. Sci.,* **2018**, *513*, 866-876, DOI: 10.1016/j.jcis.2017.12.002.

[25] Li, Q.; Xia, Y.; Yang, C.; Lv, K.; Lei, M.; Li, M., Building a direct Z-scheme heterojunction photocatalyst by $ZnIn_2S_4$ nanosheets and TiO_2 hollowspheres for highly-efficient artificial photosynthesis, *Chem. Eng. J.,* **2018**, *349*, 287-296, DOI: 10.1016/j.cej.2018.05.094.

[26] Li, C. J.; Wanga, J. N.; Wang, B.; Gong, J. R.; Lin,

Z., A novel magnetically separable TiO_2/$CoFe_2O_4$ nanofiber with high photocatalytic activity under UV-Vis light, *Mater. Res. Bulle.,* **2012**, *47*, 333-337, DOI: 10.1016/j.materresbull.2011.11.012.

[27] Salari, H.; Daliri, A.; Gholami, M. R., Graphitic carbon nitride/reduced graphene oxide/silver oxide nanostructures with enhanced photocatalytic activity in visible light, *Phys. Chem. Res.,* **2018**, *6*, 729-740, DOI: 10.22036/pcr.2018.137083.1501.

[28] Habibi-Yangjeh, A.; Golzad-Nonakaran, B., Fabrication of magnetically recoverable nanocomposites by combination of Fe_3O_4/ZnO with AgI and Ag_2CO_3: Substantially enhanced photocatalytic activity under visible light, *Phys. Chem. Res.,* **2018**, *6*, 415-431, DOI: 10.22036/pcr.2018.116937.1461.

[29] Pirhashemi, M.; Habibi-Yangjeh, A., Facile fabrication of novel ZnO/$CoMoO_4$ nanocomposites: Highly efficient visible-light-responsive photocatalysts in degradations of different contaminants, *J. Photoch. Photobiol. A: Chem.,* **2018**, *363*, 31-43, DOI: 10.1016/j.jphotochem.2018.05.027.

[30] Zarrinabadi, E.; Abghari, R.; Nazari, A.; Mirjalili, M., Environmental effects of enhancement of mechanical and hydrophobic properties of polyester fabrics using silica/kaolinite/silver nanocomposite: A facile technique for synthesis and RSM optimization, *Eurasia. J. Biosci.,* **2018**, *12*, 437-450, DOI: 10.1016/j.compositesb.2012.01.050.